Nonlinear Dynamics **24:** 373–398, 2001.

Feigenbaum Scenario Exhibited by Thin Plate Dynamics

J. AWREJCEWICZ
Department of Automatics and Biomechanics, Technical University of Łódź, Stefanowskiego 1/15, 90-924 Łódź, Poland

V. A. KRYSKO
Department of Mathematics, Saratov State University, 410054 Saratov, Russia

(Received: 19 November 1998; accepted: 11 July 2000)

Abstract. The dimensionless partial differential equations governing the dynamics of a thin flexible isotropic plate with an external load are derived and investigated. The period doubling bifurcations, as well as the chaotic dynamics, are detected and analyzed. The algorithms leading to the reduction of the original equations to those of a difference set of ordinary differential and algebraic equations are proposed, compared to other known methods, and then applied to the problem.

Among others, it is shown that, in spite of the system complexity, the Feigenbaum scenario exhibited by one-dimensional maps also governs the route to chaos in the continuous system under consideration.

Keywords: Hopf bifurcation, flexible plate, chaos.

1. Introduction

From the point of view of many engineering constructions, the nonlinear behavior of their members, such as plates and shells, is very important, and therefore has attracted the attention off researchers for a long time. In order to exhibit the nonlinear effects governed by a plate (or a shell), both single and multiple degrees-of-freedom approximation models have been studied. However, the responses of weakly nonlinear multi-degrees-of-freedom models have been investigated [1, 2]. A commonly used approach can be summarized as follows. The governing partial differential equations of the analyzed continuous system are replaced by a set of ordinary differential equations by using (in most considered cases) the Galerkin projection. Then, the obtained finite set of second-order ordinary differential equations is studied using perturbation and asymptotic analyses [3–5]. Although the possibility exists to extend the validity of these techniques to strongly nonlinear systems, for instance, by applying the ideas of Padé approximants [6], weakly nonlinear systems are primarily analyzed. There are many advantages to the afore mentioned analytical approaches. The one-mode, as well as the coupled-mode responses for both non-resonant and resonantly excited structures can be analyzed and the exchange of energy between modes can be traced. There are many papers devoted to nonlinear phenomena of thin as well as thick plates within the framework of the earlier mentioned analyses [7]. However, the perturbation and asymptotic approaches also possess some drawbacks. An initial (starting) solution to the averaging procedure does not always guarantee a required accuracy. A construction of high-order approximations is not always easy. It can also happen that the averaged amplitude differential equations are more complicated than the original equations. For instance, in [5] it has been shown that, after using the averaging procedure, the amplitudes occur in the denominators, causing serious problems

in numerically finding solutions. A further issue concerns the number of modes needed. High-mode approximations lead to very complicated averaging procedures and then a discussion of the validity of the used approximation is needed. In this paper, another approach using a difference scheme is applied. The dynamic analogue of the von Kármán partial differential equations is replaced by the second-order ordinary differential equations (ODEs) and nonlinear algebraic equations. Because a number of 256 ODEs is used (finite dimension), we put our trust in a very high approximation to the continuous system.

The stochastic behavior in deterministic systems is often realized by a framework of regular motion bifurcations which are called *bifurcation scenarios*. As has been recently explained, the process of a 'soft' occurrence of turbulence in continuous systems is related to the so-called low-dimensional chaos [8–10]. This observation implies the necessity of investigating a scenario leading to chaos in a finite-dimensioned model. The period-doubling bifurcations of periodic orbits belongs to one of the typical mechanisms realizing transition to chaos from the Morse–Smale systems to systems with chaotic behavior [11, 12].

2. Object of Analysis and Computational Algorithm

In this work, the dynamics of an elastic isotropic plate occupying, in the R^3 space, the bounded and measured (in the Lebesque sense) volume D with the boundary surface ∂D is considered. The R^3 space is parameterized using the Cartesian co-ordinate system $OXYZ$. The co-ordinate lines are attached to the midplane of the plate, whereas the OZ axis has a normal direction with a bottom sense. A surface attached to the given co-ordinate system has the form $z = 0$ and the space $\bar{D} = D \cup \partial D$ forms a cylinder of the form

$$\bar{D} = \bar{\Omega} \times \left[+\frac{h}{2}, -\frac{h}{2}\right], \quad \bar{\Omega} = \Omega \cup \partial\Omega,$$

where $\bar{\Omega} = \{x, y \mid 0 \le x \le a, 0 \le y \le b\}$ denotes a projection to the reduced surface, $\partial\Omega$ is the boundary of the reduced surface, and $\pm(h/2)$ are the front surfaces fixed on the OZ axis.

It is assumed that the plate deformations are elastic. In addition, in our considerations, the pressure in the plate layer parallel to the average surface ($OZ = 0$) is neglected. We also assume that the normal stresses σ_z in the thickness direction are much smaller compared to the stresses parallel to the reduced surface. Therefore, the following relations are valid:

$$\sigma_x^z = \frac{E}{1-\nu^2}(\varepsilon_x^z + \nu\varepsilon_y^z), \quad \sigma_y^z = \frac{E}{1-\nu^2}(\varepsilon_y^z + \nu\varepsilon_x^z),$$
$$\tau^z = \frac{E}{2(1-\nu^2)}\gamma^z, \tag{1}$$

where E is Young's modulus, ν is the Poisson coefficient, $\sigma_x^z, \sigma_y^z, \tau^z$ are the stresses in an arbitrary point of the $\bar{D}$ space with a co-ordinate z; $\varepsilon_x^z, \varepsilon_y^z$, and γ^z are correspondingly the longitudinal and rotation deformations in a plate's layer a distance z away from the reduced surface Ω. Using Kirchhoff's hypotheses, the bending deformations are governed by the relations

$$\varepsilon_{x,u} = -z\frac{\partial^2 w}{\partial x^2}, \quad \varepsilon_{y,u} = -z\frac{\partial^2 w}{\partial y^2}, \quad \gamma_u = -2z\frac{\partial^2 w}{\partial x \partial y}. \tag{2}$$

The full deformations of an arbitrary point $\varepsilon_x^z, \varepsilon_y^z, \gamma^z$ have two components. One of them is related to the reduced surface deformations

$$\varepsilon_x = \frac{\partial u}{\partial x} + \frac{1}{2}\left(\frac{\partial w}{\partial x}\right)^2, \quad \varepsilon_y = \frac{\partial u}{\partial y} + \frac{1}{2}\left(\frac{\partial w}{\partial y}\right)^2,$$

$$\gamma = \frac{\partial u}{\partial y} + \frac{\partial \upsilon}{\partial x} + \frac{\partial w}{\partial x}\frac{\partial w}{\partial y}, \tag{3}$$

whereas the second one is related to bending deformations of the form

$$\varepsilon_x^z = \varepsilon_x + \varepsilon_{x,u}, \quad \varepsilon_y^z = \varepsilon_y + \varepsilon_{y,u}, \quad \gamma^z = \gamma + \gamma_u. \tag{4}$$

In formulae (3) u, υ denote displacements of the reduced surface points in the direction of x, y. The displacements of the plate layer in the co-ordinate axes directions are the functions of the co-ordinates x, y and the time t (the same is true for deflections $w = w(x, y, t)$).

It should be emphasized that deformations in the average surface due to (3) are not independent. They are expressed by the same functions u, υ, w. Differentiating the second relation of (3) twice with respect to x, the first one with respect to y, and the third one with respect to x, y after some transformations, one obtains the following compatibility equation

$$\frac{1}{Eh}\nabla^2\nabla^2 F = -\frac{1}{2}L(w, w),$$

$$L((\cdot), (\cdot)) = \frac{\partial^2(\cdot)}{\partial x^2}\frac{\partial^2(\cdot)}{\partial y^2} - 2\frac{\partial^2(\cdot)}{\partial x \partial y}\frac{\partial^2(\cdot)}{\partial x \partial y} + \frac{\partial^2(\cdot)}{\partial y^2}\frac{\partial^2(\cdot)}{\partial x^2}. \tag{5}$$

The potential (or stress function) appearing in (5) is defined by the relations

$$N_x = \frac{\partial^2 F}{\partial y^2} - P_x, \quad N_y = \frac{\partial^2 F}{\partial x^2} - P_y, \quad N_{xy} = -\frac{\partial^2 F}{\partial x \partial y}. \tag{6}$$

In (5), L and ∇^2 are non-linear and Laplace operators, respectively.

It is necessary to append to Equation (5), the equation governing a motion of the plate's element

$$C\left[\frac{\partial^2 w}{\partial t^2} + \varepsilon\frac{\partial w}{\partial t}\right] = -D\nabla^4 w + \frac{\partial^2 w}{\partial x^2}\left[\frac{\partial^2 F}{\partial y^2} - P_x\right]$$

$$- 2\frac{\partial^2 w}{\partial x \partial y}\frac{\partial^2 F}{\partial x \partial y} + \frac{\partial^2 w}{\partial y^2}\left[\frac{\partial F}{\partial x^2} - P_y\right], \tag{7}$$

where

$$D = \frac{Eh^3}{12(1 - \nu^2)};$$

$C[\mathrm{kg/m^2}] = \rho h$ (ρ = volume density);

$\varepsilon\left[\frac{1}{\mathrm{s}}\right]$ = damping coefficient.

Equations (5) and (7) govern the motion of thin isotropic plates in a so-called hybrid form, i.e. in relation to the deflection function $w(x, y, t)$ and the stress function $F(x, y, t)$.

For the case of a stationary plate, when $w = w(x, y)$ and $F = F(x, y)$, formulae (5) and (7) were derived by von Kármán.

Using the relations

$$F = Eh^3\bar{F}, \quad x = a\bar{x}, \quad y = b\bar{y}, \quad w = h\bar{w}, \quad t = t_0\bar{t}, \quad \lambda = \frac{a}{b},$$

$$P_x = \frac{Eh^3}{b^2}\bar{P}_x, \quad P_y = \frac{Eh^3}{a^2}\bar{P}_y, \quad C = \frac{Eh^3t_0^2}{a^2b^2}\bar{C}, \quad \varepsilon = \frac{1}{t_0}\bar{\varepsilon}, \quad t_0 = T = \frac{2\pi}{\omega_0},$$

where T is the period of small free vibrations of a plate, Equations (5) and (7) are reduced to the following (bars are omitted) dimensionless form

$$\lambda^{-2}\frac{\partial^4 F}{\partial x^4} + 2\frac{\partial^2 F}{\partial x^2 \partial y^2} + \lambda^2\frac{\partial^4 F}{\partial y^4} = -\frac{1}{2}L(w, w),$$

$$C\left(\frac{\partial^2 w}{\partial t^2} + \varepsilon\frac{\partial w}{\partial t}\right) = -\frac{1}{12(1-\nu^2)}\left(\lambda^{-2}\frac{\partial^4 w}{\partial x^4} + 2\frac{\partial^2 w}{\partial x^2 \partial y^2} + \lambda^2\frac{\partial^4 w}{\partial y^4}\right)$$
$$+ \frac{\partial^2 w}{\partial x^2}\left(\frac{\partial^2 F}{\partial y^2} - P_x\right) - 2\frac{\partial^2 w}{\partial x \partial y}\frac{\partial^2 F}{\partial x \partial y} + \frac{\partial^2 w}{\partial y^2}\left(\frac{\partial^2 F}{\partial x^2} - P_y\right). \tag{8}$$

The bending moments M_x, M_y have the form

$$M_x = -\left(\frac{\partial^2 w}{\partial x^2} + \nu\lambda^2\frac{\partial^2 w}{\partial y^2}\right), \quad M_y = -\left(\frac{\partial^2 w}{\partial y^2} + \nu\lambda^2\frac{\partial^2 w}{\partial x^2}\right).$$

Equations (8) are valid for the Ω space.

Listed below are some of the boundary conditions for the edges $x = 0, 1$:

1. Free support:

$$w = \frac{\partial^2 w}{\partial x^2} = F = \frac{\partial F}{\partial x} = 0. \tag{9}$$

2. Sliding support:

$$w = \frac{\partial w}{\partial x} = F = \frac{\partial F}{\partial x} = 0. \tag{10}$$

3. Ribbed support, with the non-stretched ribs in a tangential plane:

$$w = \frac{\partial^2 w}{\partial x^2} = F = \frac{\partial^2 F}{\partial x^2} = 0. \tag{11}$$

In order to obtain the boundary conditions along two other edges $y = 0, 1$, one needs to substitute x by y in relations (9–11).

We define the following initial conditions:

$$w|_{t=0} = \varphi_1(x, y), \quad \left.\frac{\partial w}{\partial t}\right|_{t=0} = \varphi_2(x, y), \tag{12}$$

as well as the following difference operators:

$$\begin{aligned}
\lambda_x &= \frac{1}{h_x^2}[Y(x-h_x) - 2Y(x) + Y(x+h_x)],\\
\lambda_x^2 &= \frac{1}{h_x^4}[Y(x-2h_x) - 4Y(x-h_x) + 6Y(x) - 4Y(x-h_x) + Y(x+2h_x)],\\
\lambda_{xy} &= \frac{1}{4h_xh_y}[Y(x+h_x, y+h_y) + Y(x-h_x, y-h_y)\\
&\quad - Y(x+h_x, y-h_y) + Y(x-h_x, y+h_y)],\\
\lambda_{xy}^2 &= \frac{1}{h_x^2h_y^2}[Y(x-h_x, y-h_y) - 2Y(x-h_x, y) + Y(x+h_x, y-h_y)\\
&\quad + Y(x-h_x, y+h_y) - 2Y(x, y-h_y) + 4Y(x, y)\\
&\quad - 2Y(x+h_x, y) + Y(x, h_x, y+h_y) - 2Y(x, y+h_y)],
\end{aligned} \tag{13}$$

where Y is represents either $w(x, y)$ or $F(x, y)$, respectively, whereas h_x and h_y correspond to the spatial steps in the direction of x and y, respectively.

Therefore, the partial differential equation (PDE) is reduced to that of differential algebraic equations (DAEs) for the stress function F and the deflection function w, correspondingly:

$$\begin{aligned}
&C(\ddot{w}_{i,j} + \varepsilon\dot{w}_{i,j}) = -\{A(w) + B(w, F) - H(w)\},\\
&D(F) = E(w),
\end{aligned} \tag{14}$$

where

$$\begin{aligned}
A(w) &= \frac{1}{12(1-\nu^2)}(\lambda^{-2}\lambda_x^2 w_{ij} + 2\lambda_{xy}^2 w_{ij} + \lambda^2\lambda_y^2 w_{ij}),\\
B(w, F) &= \lambda_x w_{ij}\lambda_y F_{ij} + \lambda_y w_{ij}\lambda_x F_{ij} - \lambda_{xy} w_{ij}\lambda_{xy} F_{ij},\\
H(w) &= \lambda_x w_{ij} P_x + \lambda_y w_{ij} P_y,\\
D(F) &= 12(1-\nu^2)A(F),\\
E(w) &= -\lambda_x w_{ij}\lambda_y w_{ij} + [\lambda_{x,y} w_{ij}]^2.
\end{aligned} \tag{15}$$

The resulting system of second-order differential equations (ODEs) involving the variable

$$\frac{\mathrm{d}w_{ij}}{\mathrm{d}t} = w'_{ij} \tag{16}$$

reduces to ODEs of the first order in relation to time for deflections w_{ij} and their velocities w'_{ij} and to the AEs for the stress function F_{ij}:

$$C\left(\frac{\mathrm{d}w'_{ij}}{\mathrm{d}t} + \varepsilon w_{ij}\right) = -\{A(w) + B(w, F) - H(w)\}, \tag{17}$$

$$D(F) = E(w). \tag{18}$$

In order to solve Equations (16–18) with the initial conditions (12) using one of the boundary conditions (9–11) the following algorithm is applied:

1. The initial deflection values in each of the finite-difference mesh nodes are substituted in the right-hand side of the AEs (18), and then the corresponding stress function F_{ij} field is obtained using the Gauss method.
2. The obtained stress function values F_{ij} are substituted into the right-hand side of the ODEs (16) and (17), which are integrated using the Runge–Kutta method. As a result, fields of deflections w_{ij} are obtained in the next time step.

As has already been mentioned, the AE system is solved using the Gauss method in relation to the stress function F_{ij}. A choice of that method is implied by an observation that the system of algebraic equations is solved for each time step, but a matrix of the system is unaltered (only the right-hand sides are changed). This is an important property because that matrix can be reduced to a triangular form only once at the first time step. As has been pointed out in [13], the described procedure leads to a reduction in the number of computations of at least 5 in comparison to the classical iteration method.

The ODEs are integrated using the fourth order Runge–Kutta method. A solution to the discussed problem can be found with the largest step within the framework of a numerically stable solution.

The necessary requirement from the point of view of computations depends on the operational memory and computation speed. For instance, if the investigated space is divided for $N = n \times n$ points, then at each time step we need to solve k times (k is the order of the Runge–Kutta method) the system of algebraic equations with the $n \times n$ matrix. A fundamental part of the computational time is used to solve the linear algebraic equations. However, we are also able in this case to decrease the computational time. Assuming that during each step of computations the stress function is only slightly changed, we need to solve Equation (16) only once. However, some limitations still exist from a point of view of system memory. During application of the Gauss method we need to be aware of the $n \times n$ matrix. It is especially important when a dynamical problem is solved within the large time intervals.

3. Analysis

In order to estimate the efficiency and reliability of the proposed algorithm, the results will be compared with those obtained using other methods.

For test purposes, we take a series of known problems. First, we calculate the first critical loads for $\lambda = a/b = 1$ for plates subjected to a constant stretching load $P_x (P_y = 0)$. The critical loads are determined using the dynamical excitation. The latter has been defined using initial conditions of the form

$$w|_{t=0} = A_H \sin mx \sin ny,$$

$$\dot{w}|_{t=0} = 0.$$

Then, the ODEs governing a dynamical plates behavior with a surrounding medium damping $\varepsilon = \varepsilon_{cr}$ are analyzed ($\varepsilon = \varepsilon_{cr}$ denotes a critical damping value, for which the vibrations vanish). On a basis of the obtained solution, one can judge the character of the acting load.

If a driven load is smaller than the critical one, then a solution to the dynamical problem approaches a stationary state equal to zero: $\lim_{t\to\infty} w(t, x, y) = 0$.

If a load is larger than the critical value, then a stationary solution is different from a linear equilibrium. It should be noted that a statical solution property for a load near, below, and

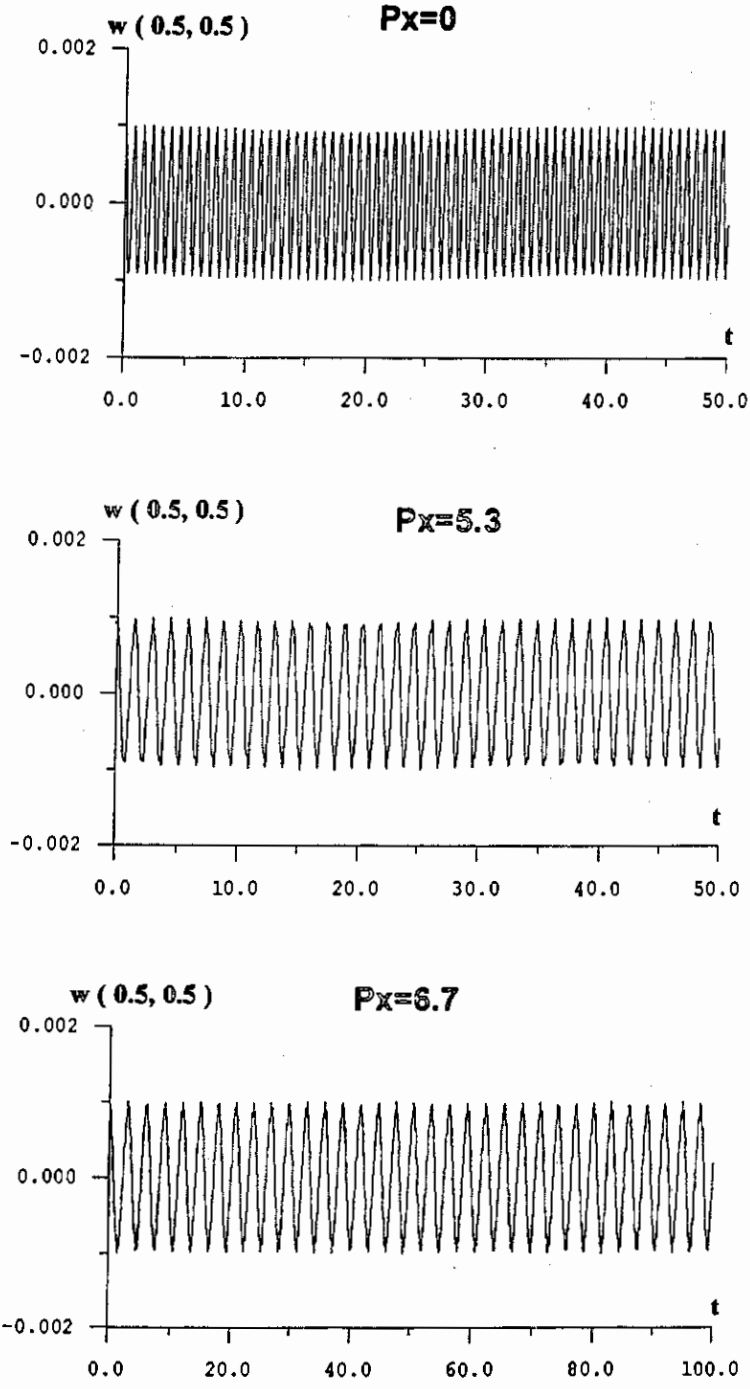

Figure 1a. Time histories related to the plate centre for different P_x load values.

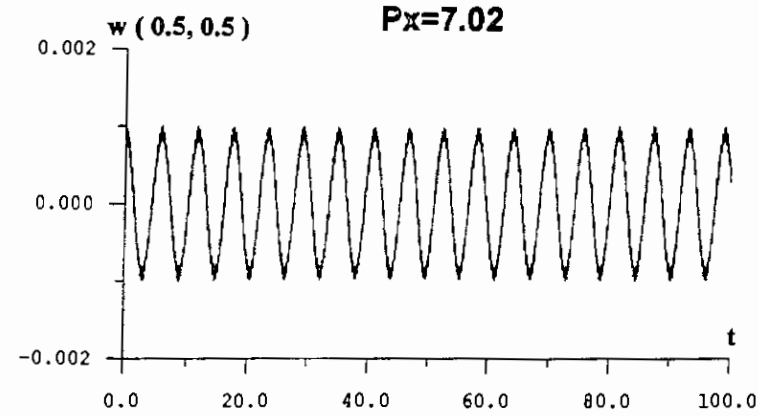

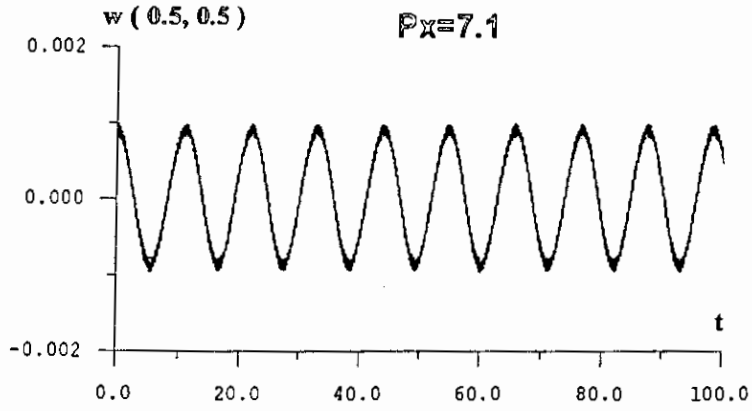

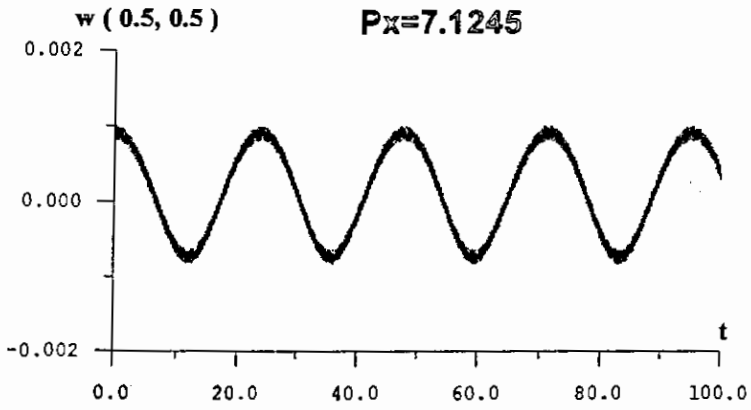

Figure 1b. Continued.

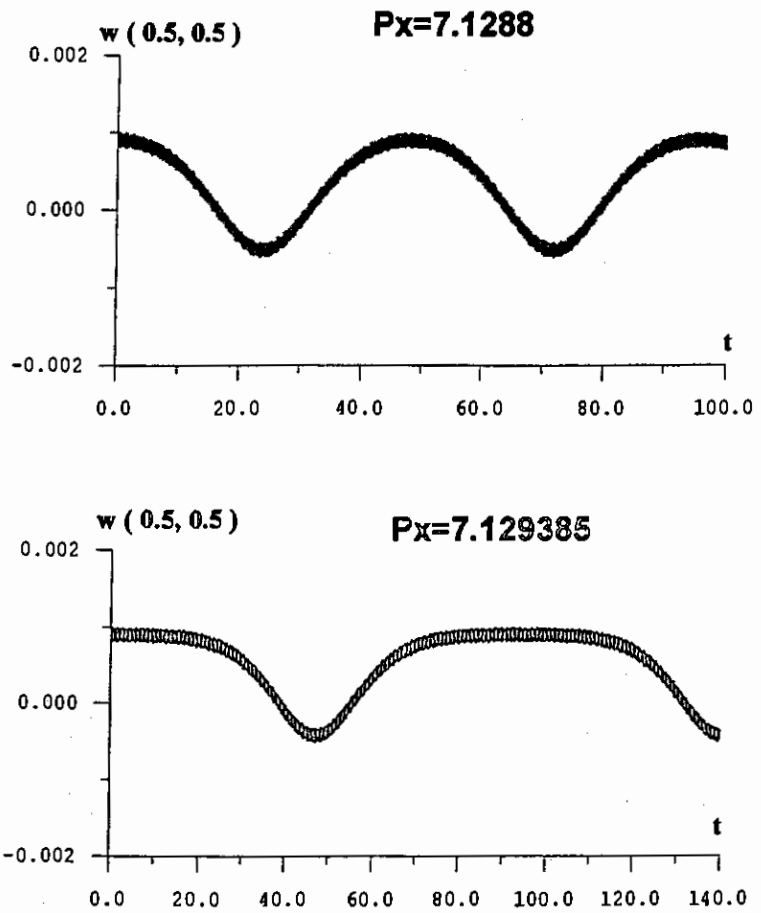

Figure 1c. Continued.

Table 1. Critical load values obtained using different computational methods.

No	Boundary conditions		
	(8)	(9a)	(10)
1	3.60	9.21	–
2	3.48	8.40	–
3	3.61	9.12	3.61

above the critical values does not depend on the choice of the initial conditions. The damping coefficient ε helps us to reach a stationary state and does not influence the kind of statical solution.

In Table 1, the critical load values obtained by using different methods for plates with the afore-mentioned boundary conditions (9, 10) and (11) are presented.

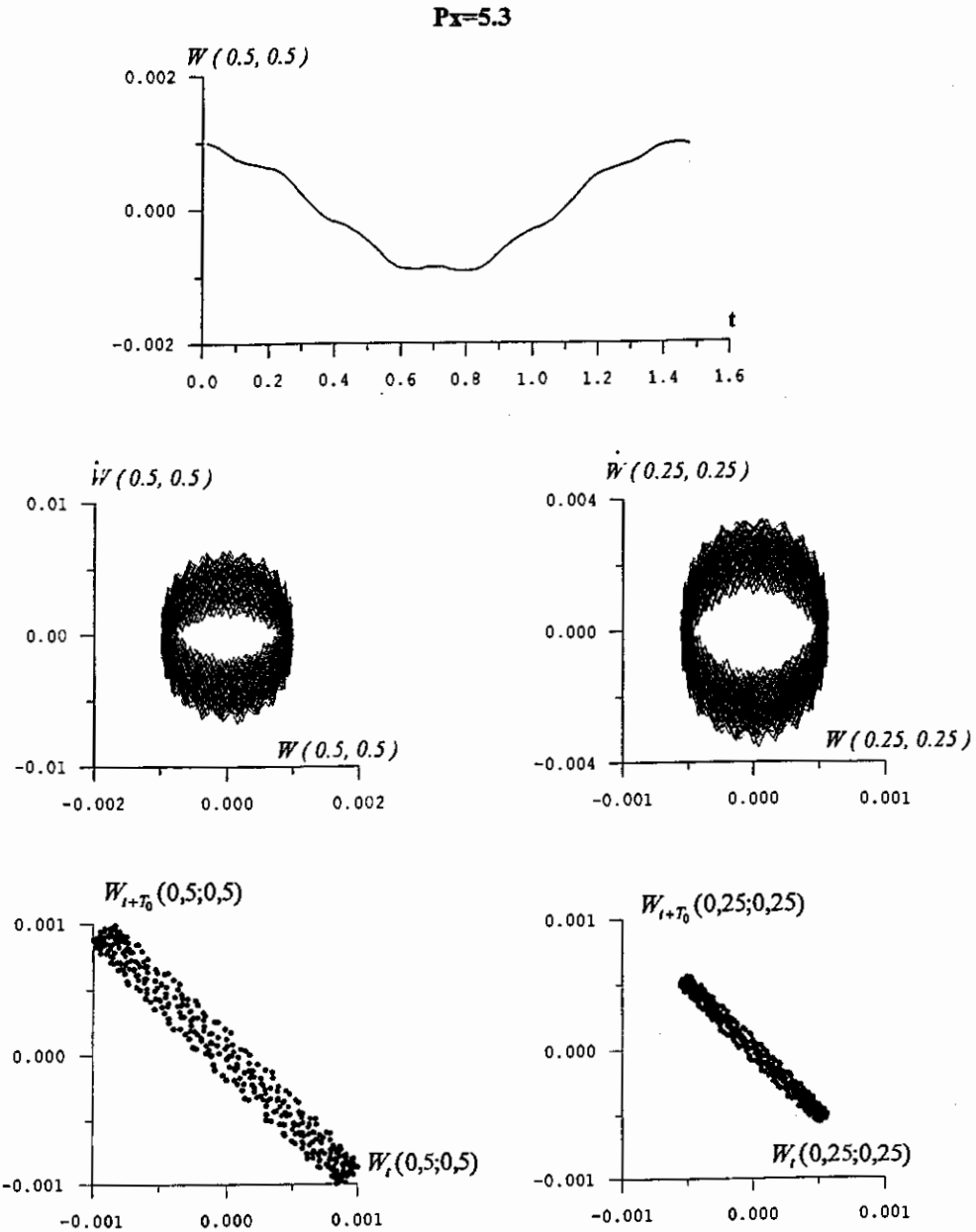

Figure 2a. Time histories, phase projections and Poincaré maps for $w(0.5; 0.5)$ and $w(0.25; 0.25)$ and for diffcrent P_x load values: (a) 5.3; (b) 6.7; (c) 7.02; (d) 7.1; (e) 7.1245; (f) 7.1288; (g) 7.129385; (h) 7.129406; (j) 7.129406, $t \in [0.37]$; (k) 7.129406, $t \in [0.60]$; (l) 8.

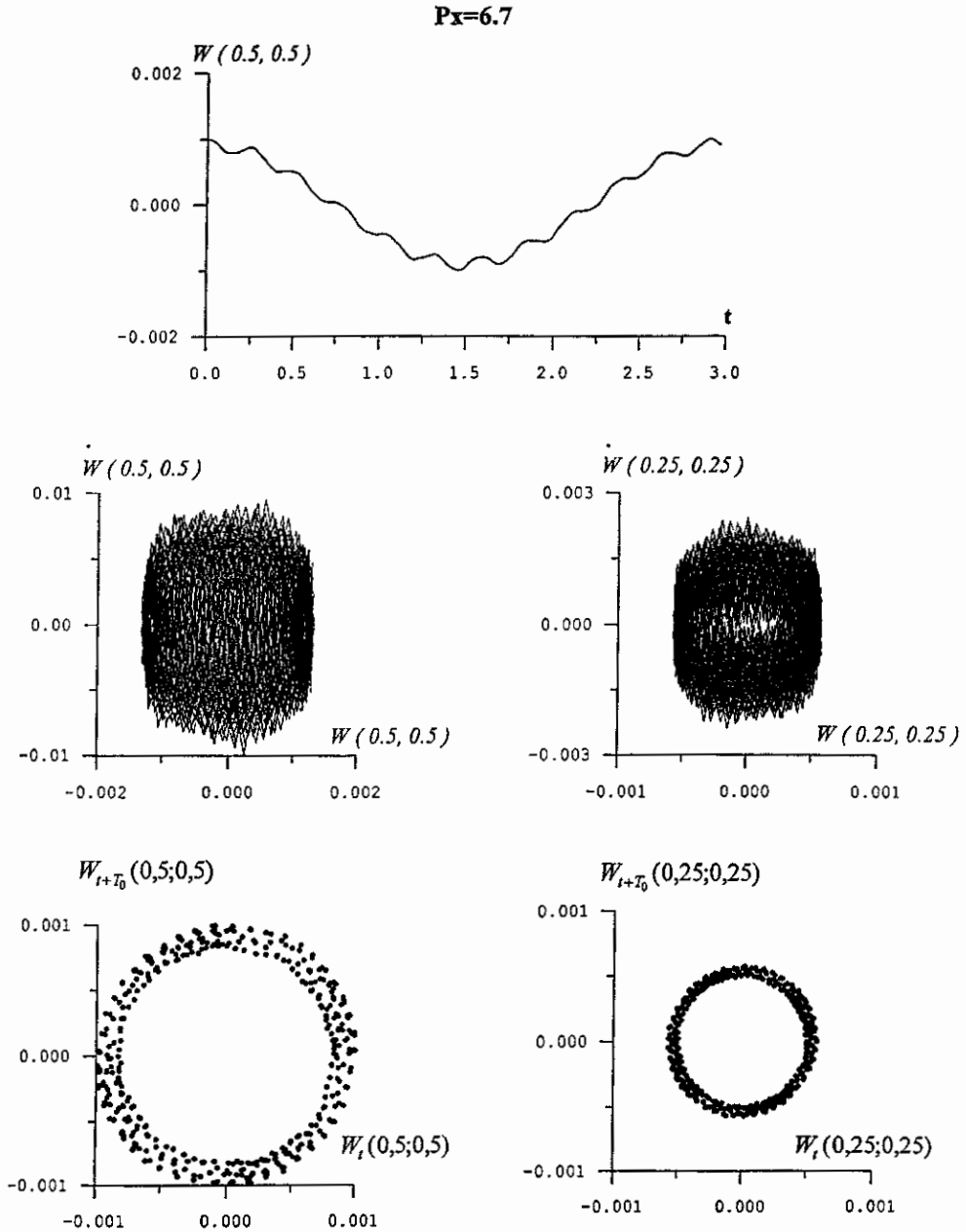

Figure 2b. Continued.

In row 1, the critical loads obtained by using the spectral methods are given [13]. In row 2 the solution obtained by using the finite difference method in combination with a method of sequentially applied loads is given [14]. In row 3, the solutions obtained using a relaxation method by a partition into 16 × 16 parts of the plate are used.

It is clearly seen that a solution obtained using the relaxation method fully overlaps with that obtained using the spectral method. Besides, the boundary conditions for the stress function F do not influence the value of the critical load (1st and 3rd rows of Table 1). Therefore,

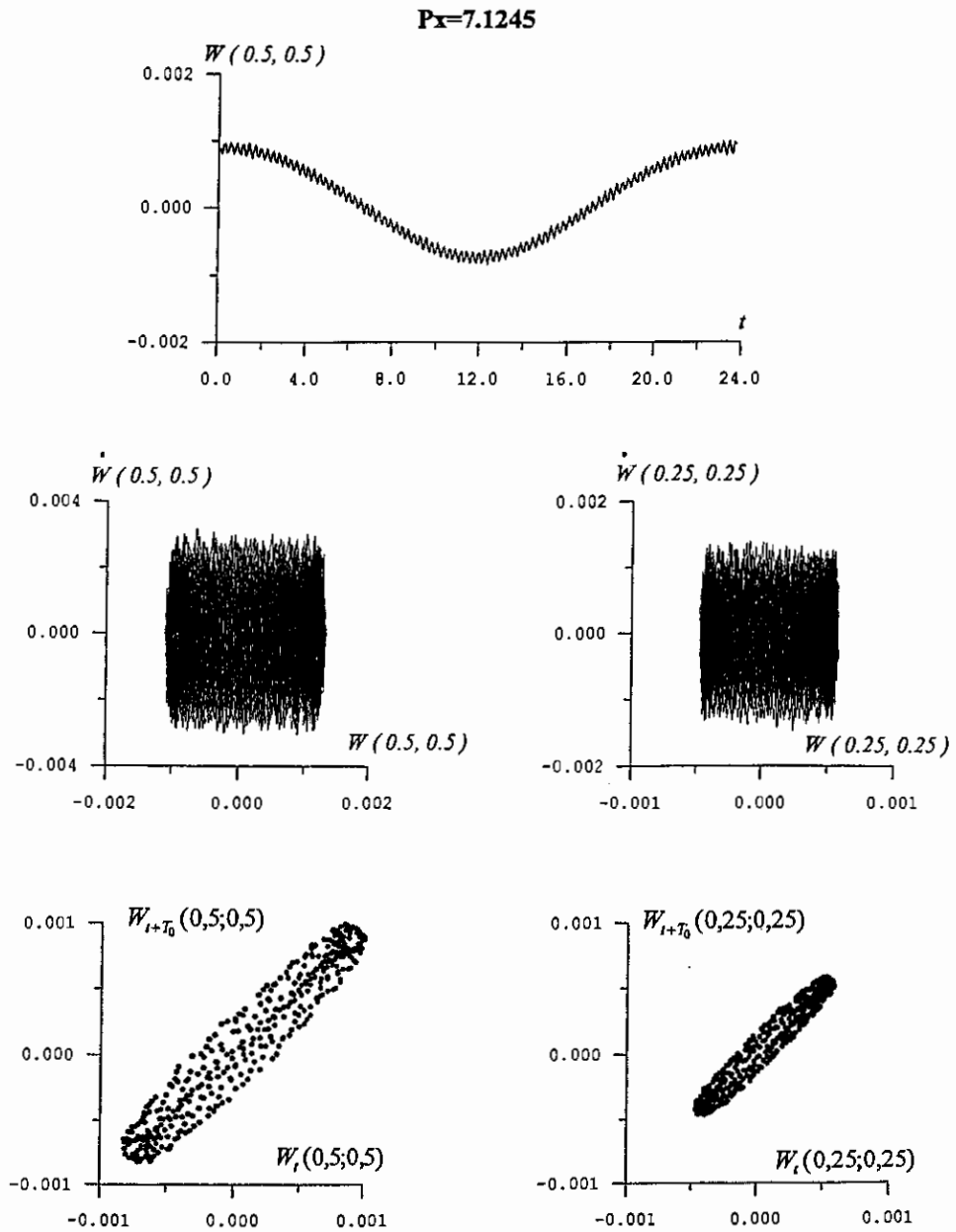

Figure 2c. Continued.

in order to detect the first critical load of rectangular plates, a linear statement of the problem can be used.

Stochasticity in a deterministic systems can be realized by a bifurcation scenario.

An occurrence of a weak turbulence in a continuous systems is related to low-dimensional chaos, which stimulated further investigations of stochastic behavior in the finite-dimensional models [15–17]. Typical mechanisms that are responsible for the transition from the Morse–

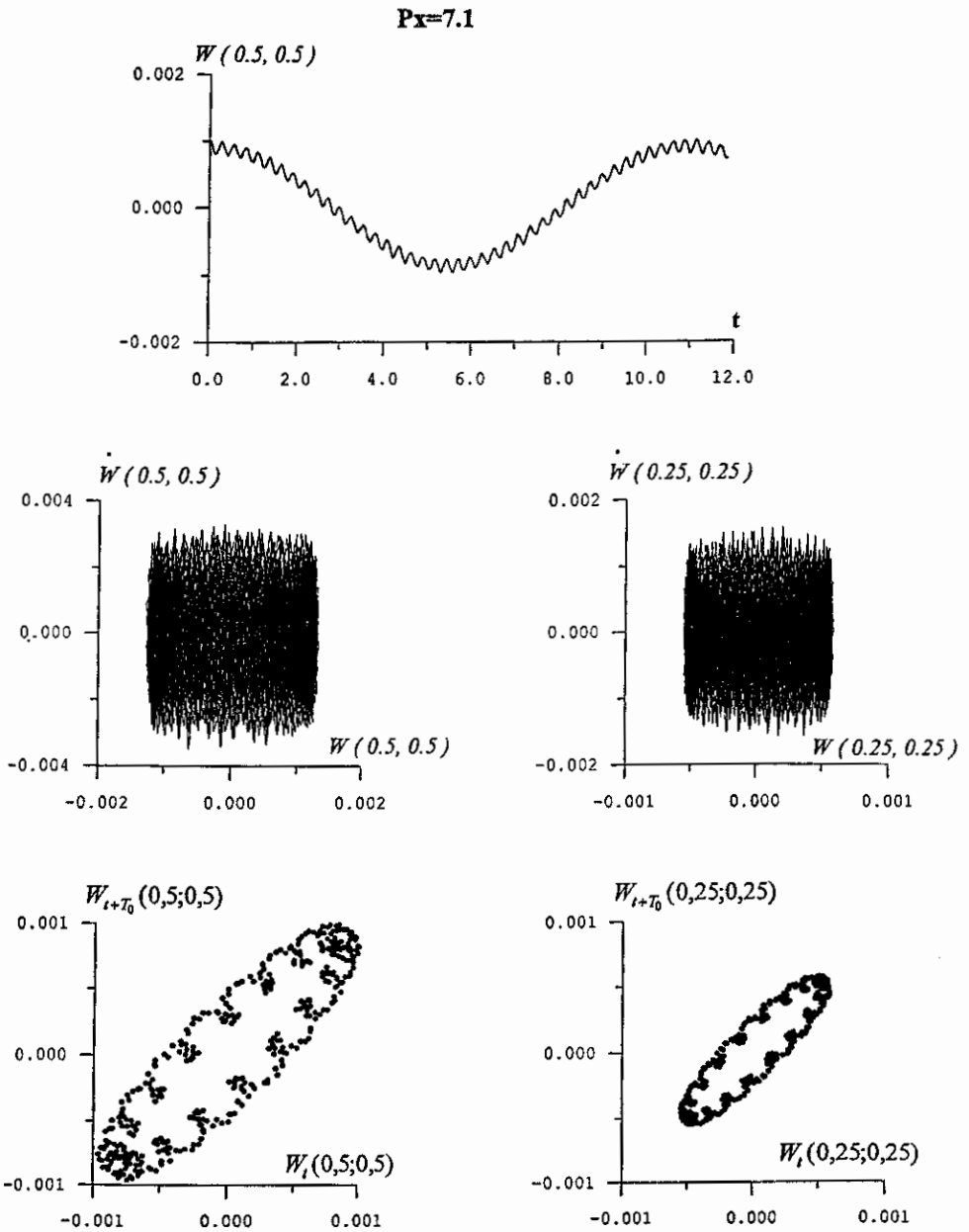

Figure 2d. Continued.

Smale systems to those with chaotic motion include scenarios of infinite sequence of period-doubling bifurcations.

In the vicinity of the critical point and assuming that the contraction in each directions is higher than the expansion (locally occurring only in one direction), a transition can be described using a one-dimensional map.

We illustrate and analyze the transition to chaos by period-doubling the bifurcations on the example of the squared free supported plate (boundary condition (9), $\lambda = a/b = 1$). The

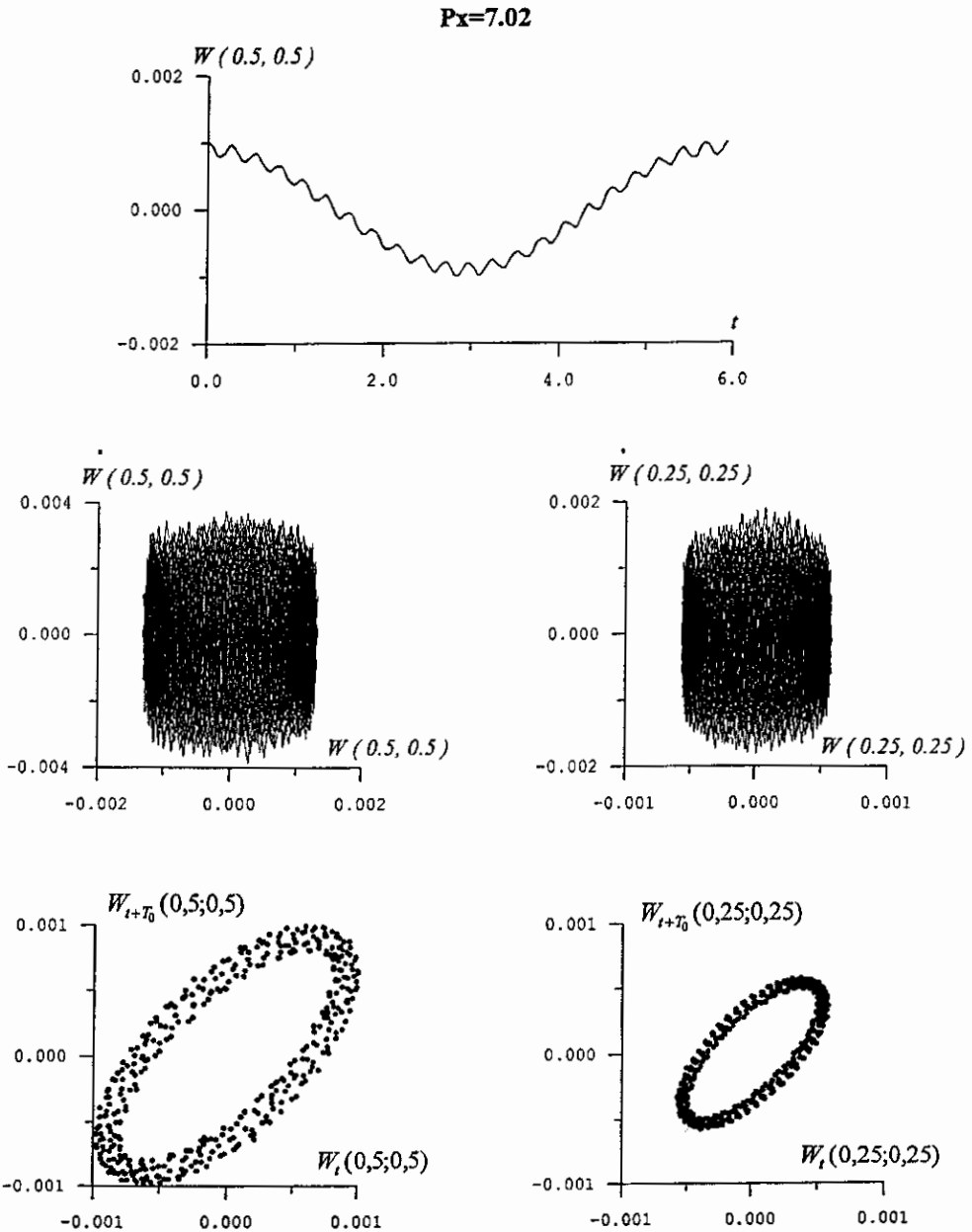

Figure 2e. Continued.

longitudinal load (P_x) acts along the sides $x = 0$, $x = 1$ ($P_x = 0$), and the earlier-mentioned initial conditions are applied.

A convergence of the computational process in time and space co-ordinates has been examined by using the Runge principle. The time step $\Delta t = 0.0025$, as well as the space co-ordinate step 16×16 is used.

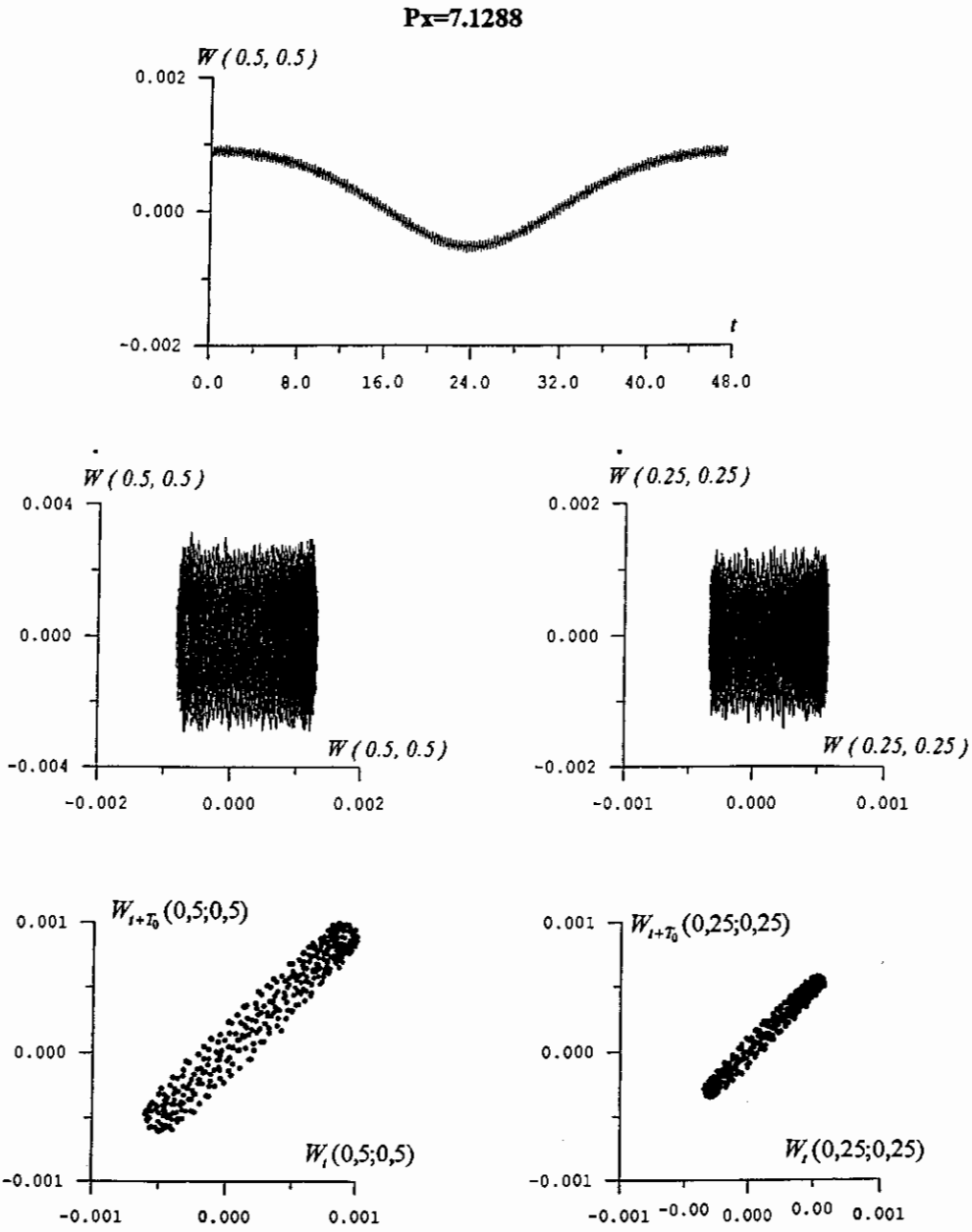

Figure 2f. Continued.

Before the stationary state loses its stability, the basin of attraction becomes very small and perturbations throw the state of the system from that basin even before attraction property fully vanishes.

This behavior is related to the so-called stiff stability loss. The mechanical systems state leaves the stationary state by jumps to a different state. The new state can be a stationary one, characterized by a more complex behavior. The existing dynamical stability criterions applied to plates are given in [18–20].

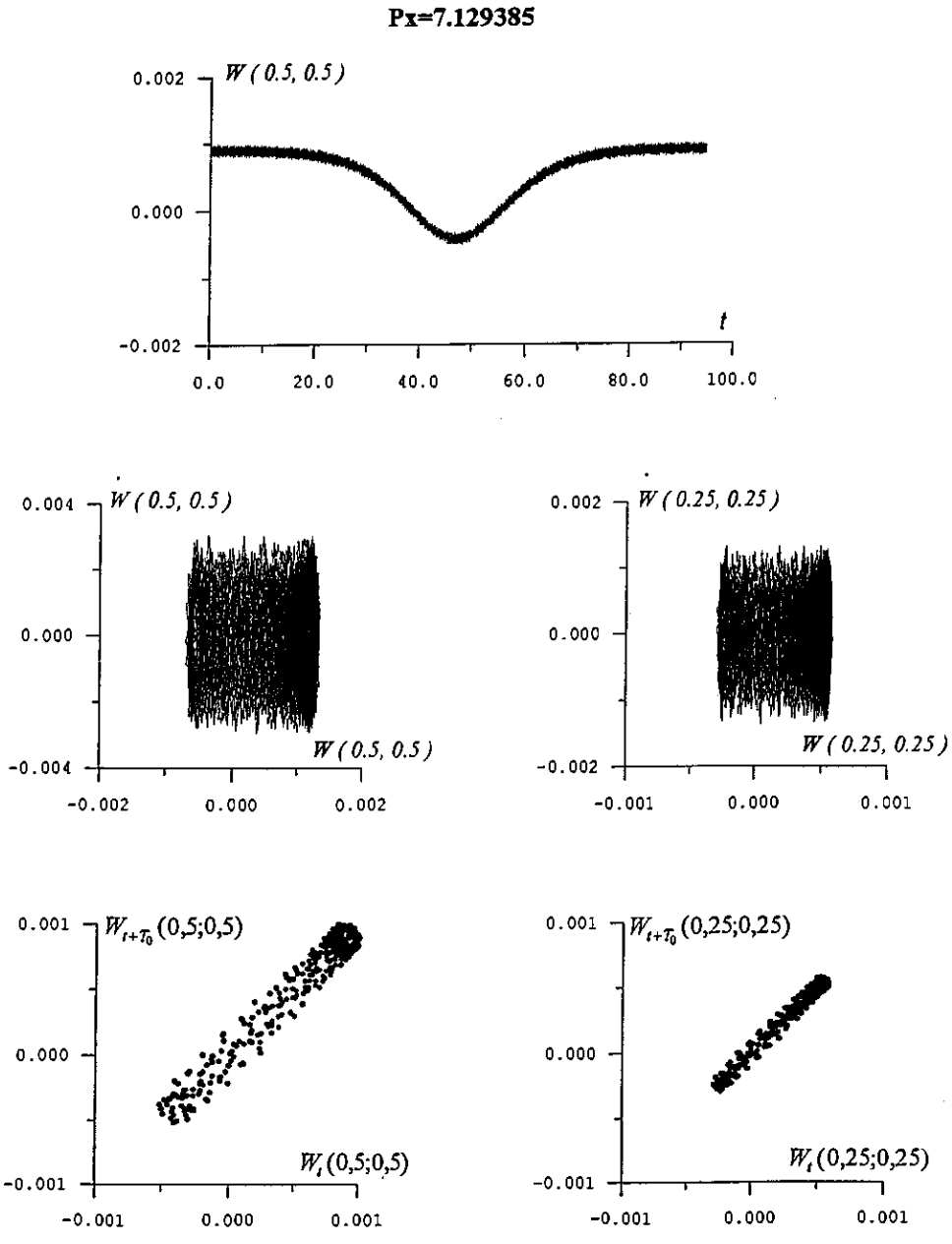

Figure 2g. Continued.

4. Discussion and Conclusions

Consider a stiff stability loss of the squared plate in relation to the longitudinal load P_x further considered as a control parameter. The Hopf bifurcation sequence is analyzed.

In Table 2, a dependence of P_x for two initial exciting amplitudes ($A_H = 0.001$ and $A_H = 0.3$) is reported. The P_x value below the marked horizontal line corresponds to the stiff stability loss. Below, the results for $A_H = 0.001$ will be given.

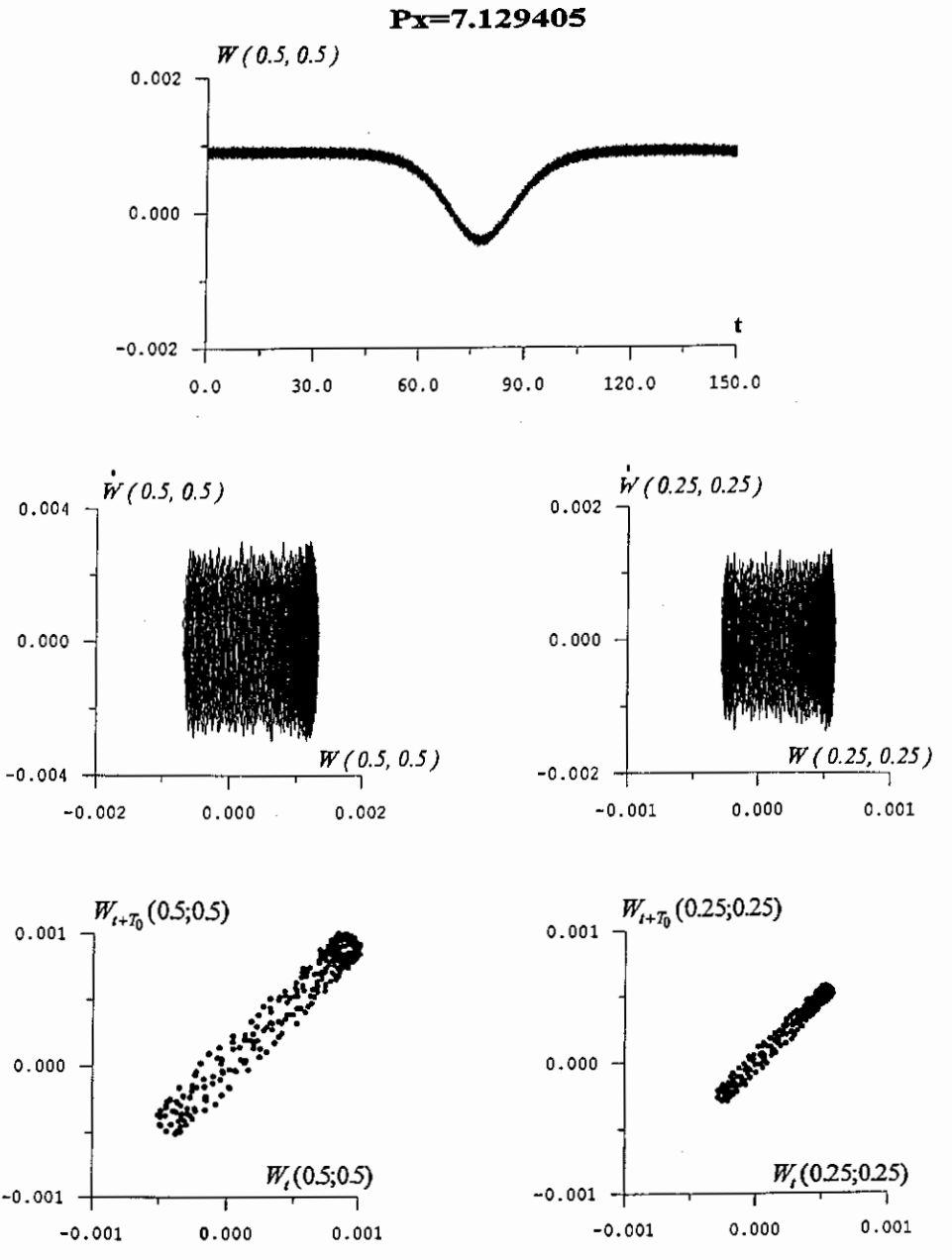

Figure 2h. Continued.

In Figure 1, vibrations of the plate centre deflection ($w(0.5; 0.5)$) *versus* time for free ($P_y = 0$) and applied loads corresponding to the first, second, ..., seventh Hopf bifurcations are given. The corresponding load values are shown in the corresponding drawings in Figure 1.

The qualitative changes of the system states are presented in Figures 2a–2l. On each figure, the time histories $w(t)$ of the plate's centre (one halfperiod), phase portraits $\dot{w}(w)$, and Poincaré mapping $w_{t+t_0}(w)$ for $w(0.5; 0.5)$ and $w(0.25; 0.25)$ are reported.

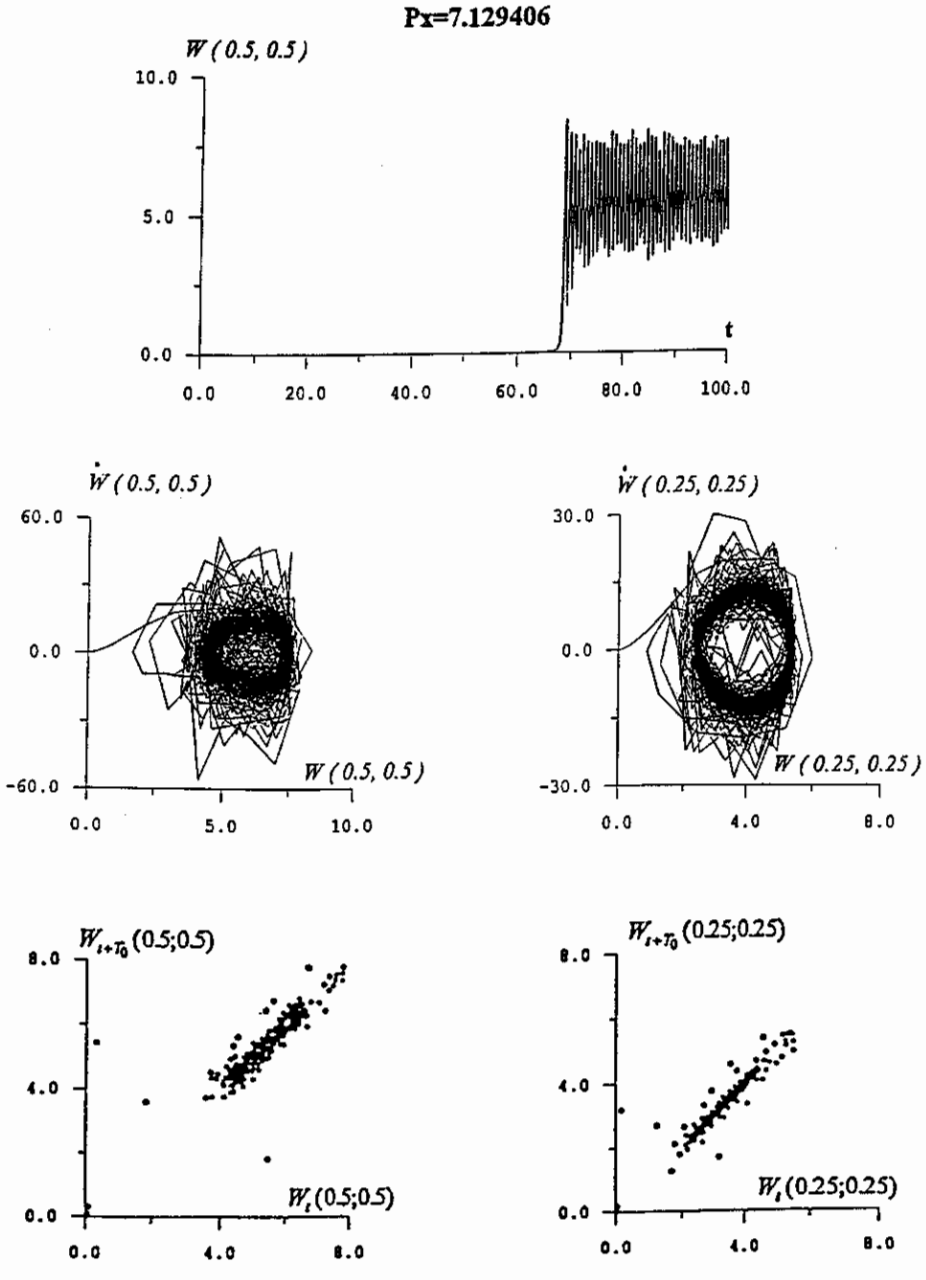

Figure 2i. Continued.

A convergence of a sequence of bifurcation values P_{x_k} and P_{x^*} are characterized by

$$\delta = \frac{P_{x_{k+1}} - P_{x_k}}{P_{x_{k+2}} + P_{x_{k+1}}}.$$

With an increase of k, the value of δ_k does not depend on k and converges to the constant

$$\delta = \lim_{k \to \infty} \delta_k = 4.669201 \ldots$$

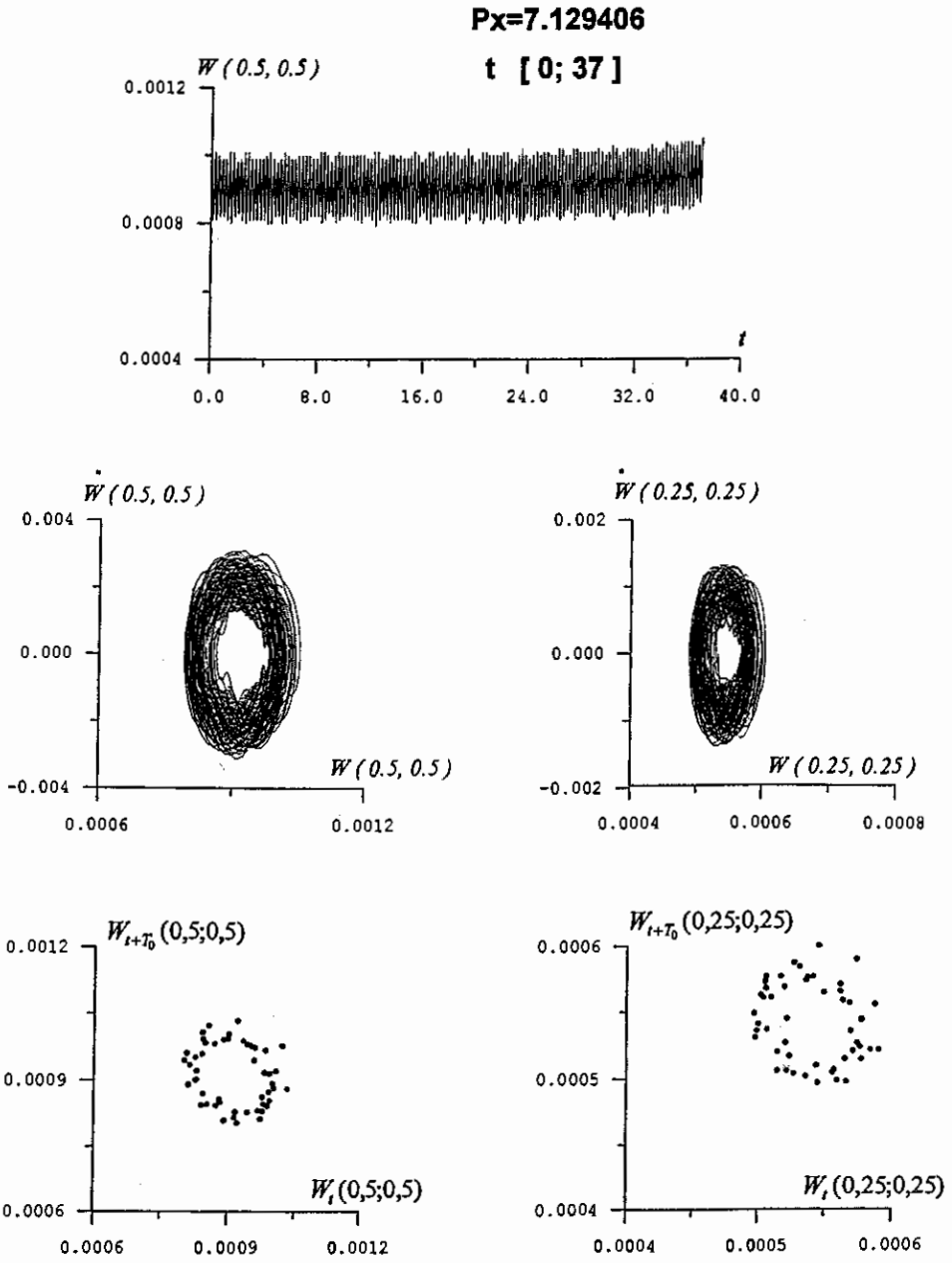

Figure 2j. Continued.

This Feigenbaum constant describes a convergence velocity of the bifurcation parameter $P_{x_k} \to P_{x^*}$.

The Poincaré mapping for free vibrations consists of the straight line part sloped to the horizontal axis of 45°. The phase portrait corresponds to an ellipse. After the first period doubling ($P_{x1} = 5.3$, Figure 2a), the Poincaré section rotates by 90°, becomes broader and

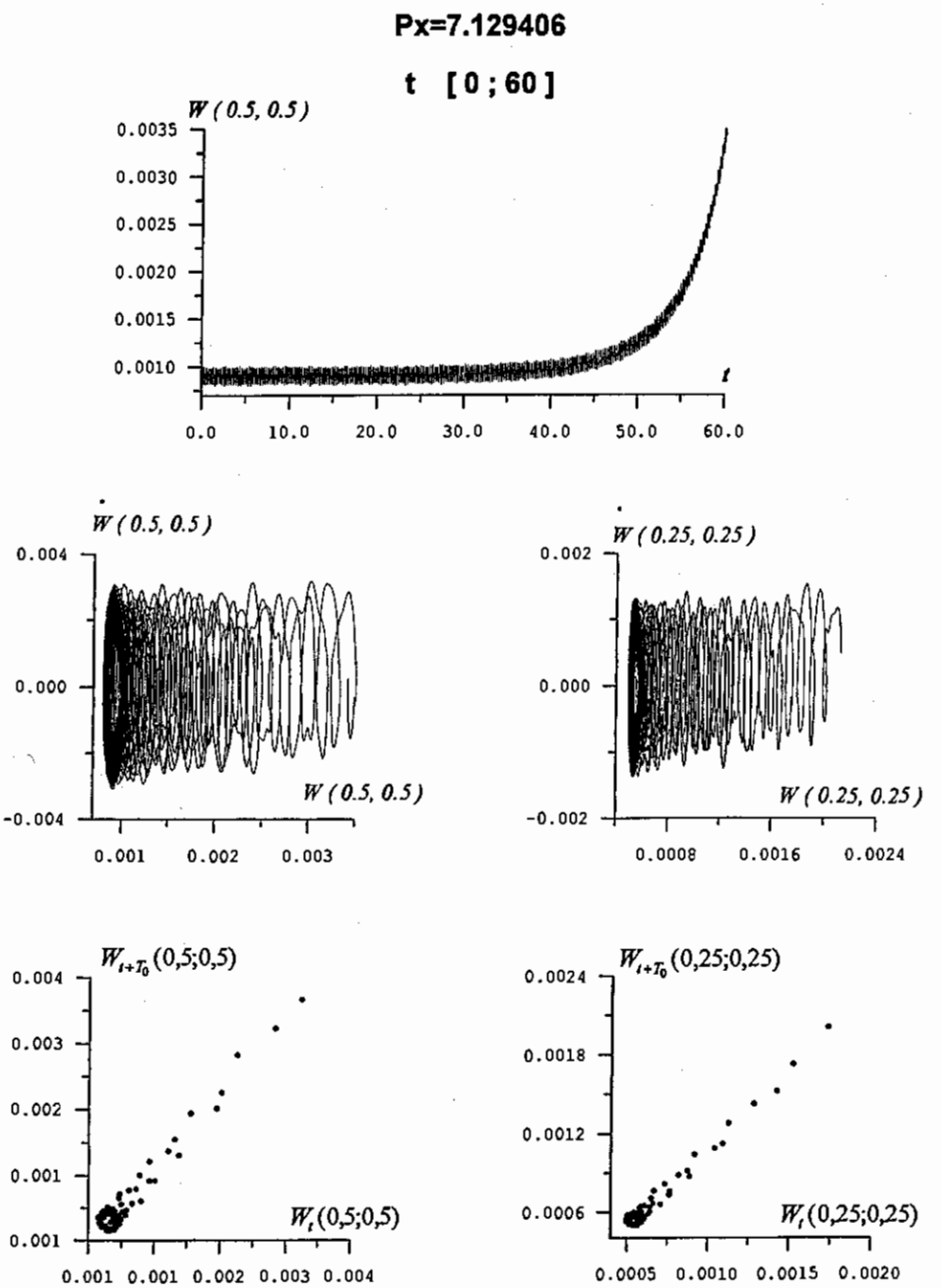

Figure 2k. Continued.

is sloped at approximately 135° to the horizontal axis. A velocity change is observed in the phase portrait.

For $P_{x2} = 6.7$ (Figure 2b – second Hopf bifurcation) in the Poincaré section, the strange attractors occur as a result of the occurrence of weak orbits having a circle shape in the transversal cross-section. Much higher velocities are observed. The phase portraits and the Poincaré mapping are similar for every plate point.

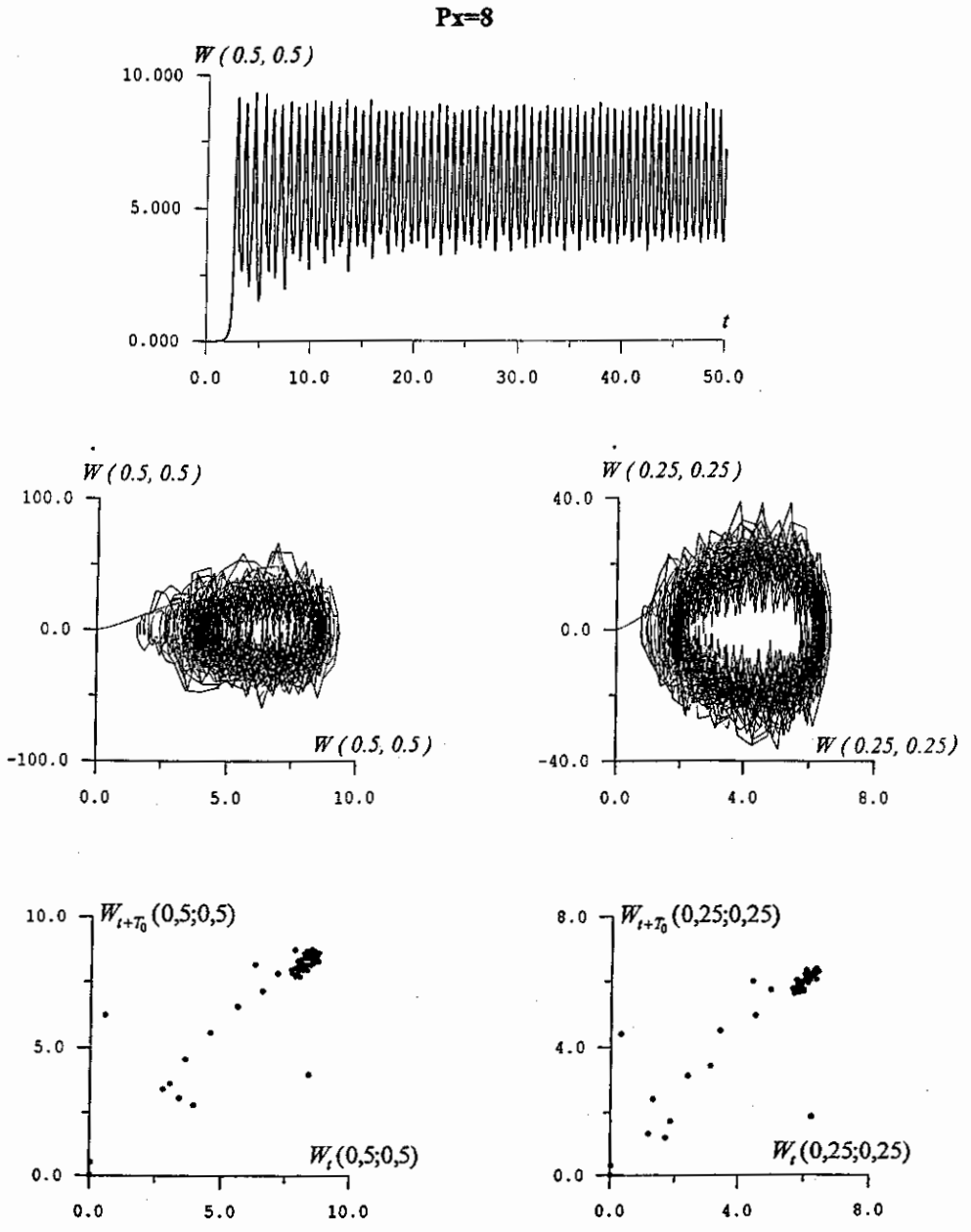

Figure 2l. Continued.

Looking for further values of the bifurcation parameter $P_{xk}(k = 3, 4, 5, 6, 7)$, it is seen that a sequence $\{P_{xk}\}$ converges to the critical point $P_{x^*} = 7.129405$. Beginning from the third Hopf bifurcation, a cross-section of the Poincaré map has an elliptic form, the larger axis of which is sloped by 45° to the horizontal axis. After the fourth Hopf bifurcation, an orbit cross-section possesses a complex form exhibiting a kneading phenomenon. These kneading effects increase with the increasing number of Hopf bifurcation. A period of 'noisy' components

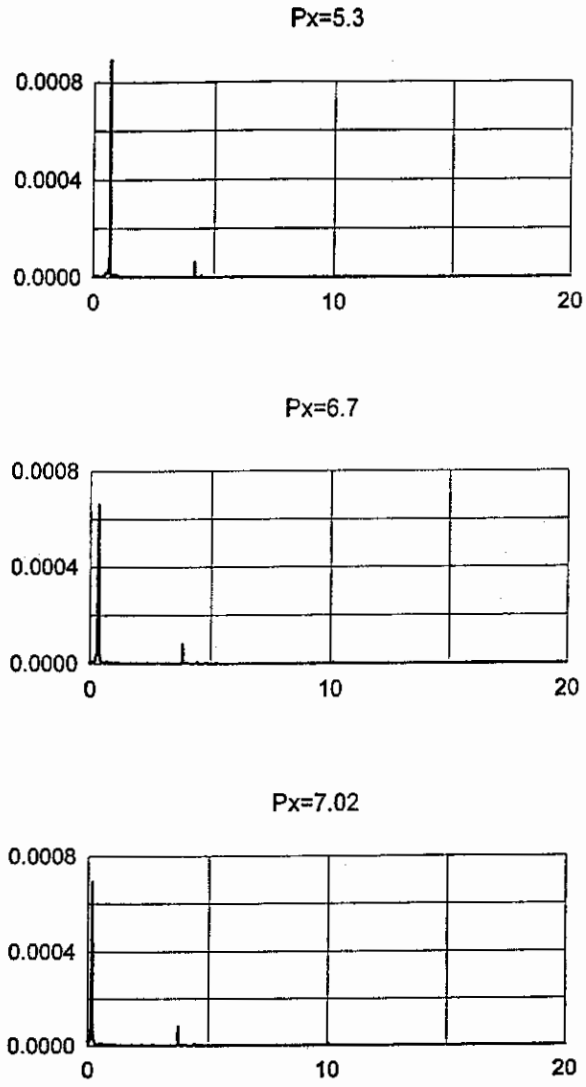

Figure 3a. Power spectra for different P_x load values.

decreases and a basin of attraction occurs, which is demonstrated on the phase portraits and the Poincaré sections (the right-hand parts of drawings $w_{t+t_0}(w_t)$ and $\dot{w}(w)$, see Figures 2f–2h).

Similar information is also exhibited in Figure 2h for $P_x = 7.129405$. A change of P_x for 1×10^{-6} leads to a stiff stability loss ($P_{x^*} = 7.129406$). The system has achieved another state by a jump.

In this case, the time of a stiff stability loss occurrence belongs to the largest one. It means that the stability loss occurs with a very slow change of the parameter. Even for the critical P_{x^*} value, a dynamical stability loss plays a secondary role for $t < t_{cr}$, i.e. before an occurrence of a stiff stability loss. In Figure 2j ($t \in [0, 60]$), an evolution of a transitional state to a new one is presented (in the phase portrait the prehistory of the systems motion is given). In the time interval $t \in [0, 37]$, a closed motion trajectory, rotating around the corresponding stable equilibrium, is observed. When a longer time interval is analyzed, $t \in [0, 60]$, a transition to

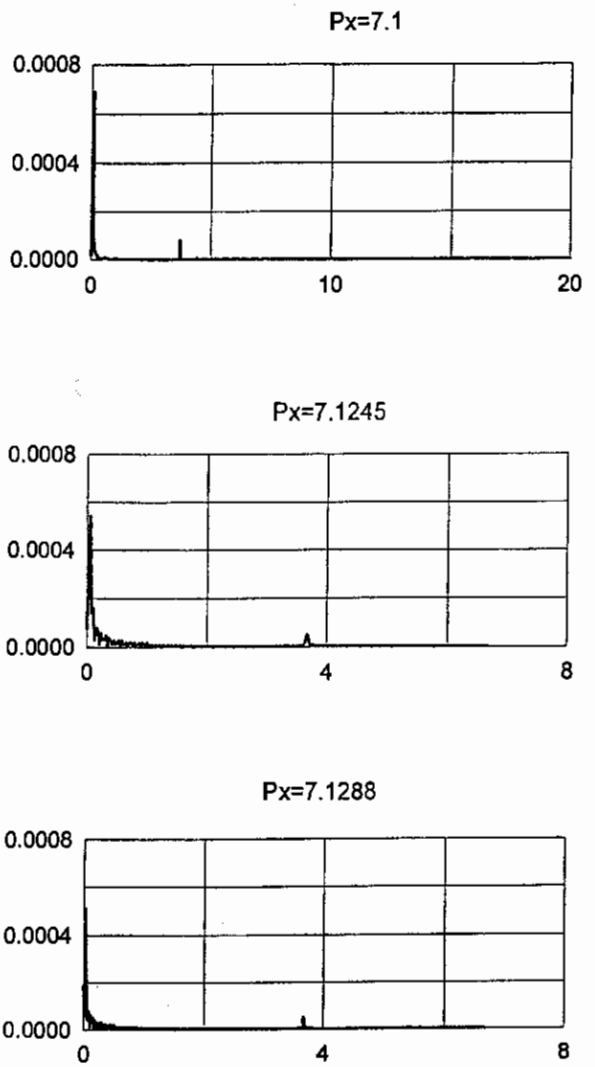

Figure 3b. Continued.

a new dynamical state is outlined, which can be followed using the Poincaré section. With an increase of P_x, the time of transition to a new dynamical state decreases (Figure 2l, $P_x = 8$) and some of the attracting orbits die.

The frequency spectra for the mentioned Hopf bifurcations are given in Figure 3 with the corresponding compressing impulse values P_x with infinite duration in time. The Hopf bifurcation corresponds to two fundamental frequencies. Beginning from the fifth Hopf bifurcation ($P_x = 7.1245$), an amplitude and number of periods of noisy state increase. Let us focus on the cases of $P_x = 7.129405$ and $P_x = 7.129406$. A change of P_x of 1×10^{-6} leads to significant qualitative and quantitative changes. The broad band spectrum is presented for $P_x = 7.129406$.

To conclude, a qualitative picture of dynamical plate behavior is similar to that of its centre. A number of Hopf bifurcations depend on the initial excitation amplitude A_H. An increase of

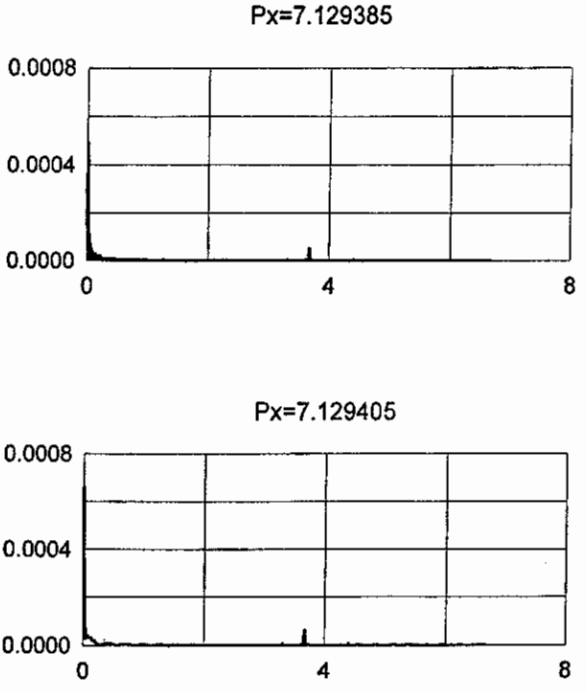

Figure 3c. Continued.

Table 2. A sequence of Hopf bifurcation.

Hopf bifurcation number	A_H	
	0.001	0.3
	P_x	
1	5.3	5.0
2	6.7	6.3
3	7.02	6.431
4	7.1	6.4315
5	7.1245	
6	7.129385	
7	7.129385	

A_H accompanies a decrease in the number of Hopf bifurcations to three ($A_H = 0.3$) and two ($A_H > 0.3$). A chaotic attractor occurs for larger A_H.

In an analogous way, the pictures for the stress function $F(x, y, t)$, the membrane stresses $N_x = \partial^2 F/\partial y^2$, $N_y = \partial^2 F/\partial x^2$, and the moments M_x, M_y, can be constructed, illustrating a similar behavior.

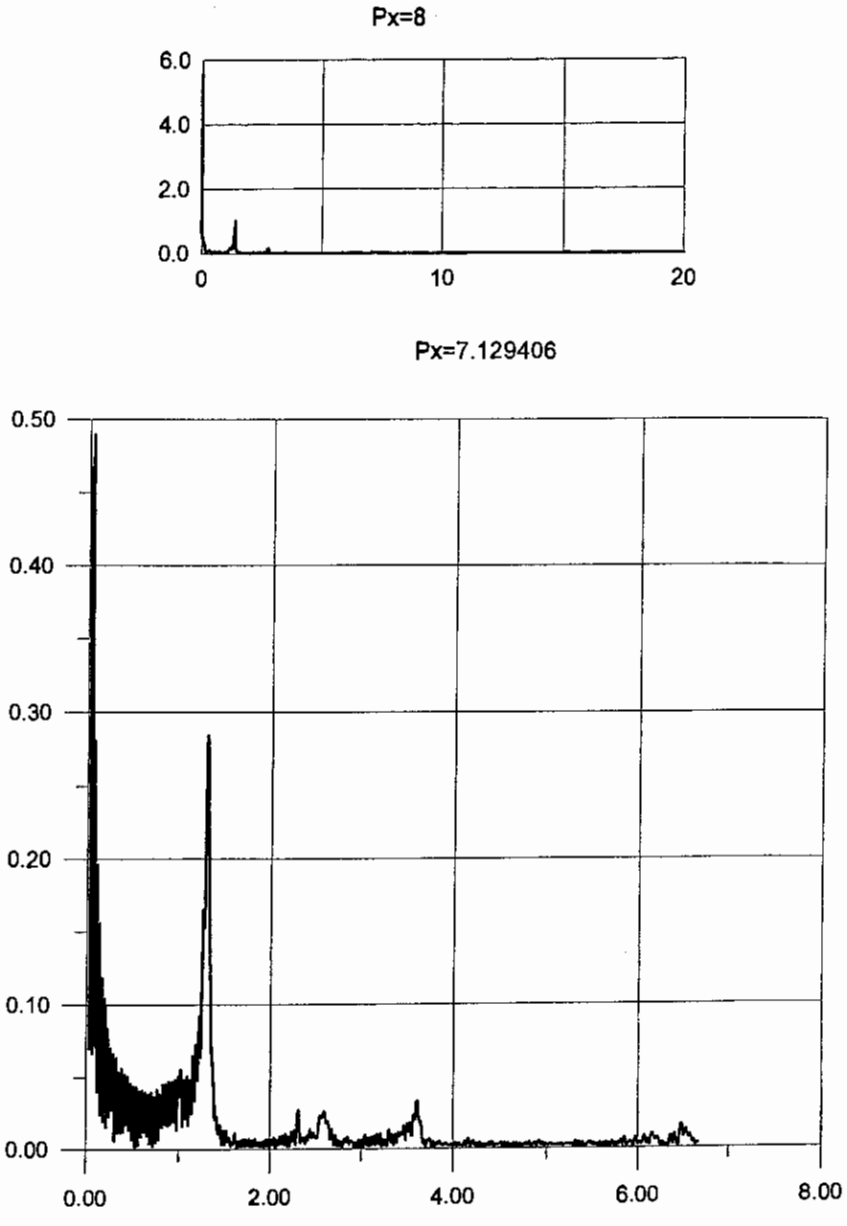

Figure 3d. Continued.

References

1. Nayfeh, A. H. and Mook, D. T., *Nonlinear Oscillations*, Wiley-Interscience, New York, 1979.
2. Chang, S. I., Bajaj, A. K., and Davies, P., 'Bifurcations and chaotic motions in resonantly excited structures', in *Bifurcation and Chaos-Theory and Applications*, J. Awrejcewicz (ed.), Springer-Verlag, Berlin, 1995, pp. 217–249.
3. Nayfeh, A. H. and Balachandran, B., 'Modal interactions in dynamical and structural systems', *Applied Mechanics Review* **42**, 1989, 5175–5201.

4. Johnson, J. M. and Bajaj, A. K., 'Amplitude modulated and chaotic dynamics in resonant motion of strings', *Journal of Sound and Vibration* **128**, 1989, 87–107.
5. Awrejcewicz, J., 'Strange nonlinear behavior governed by a set of four averaged amplitude equations', *Meccanica* **31**, 1996, 347–36.
6. Thompson, J. M. T. and Stewart, H. B., *Nonlinear Dynamics and Chaos*, Wiley, Chichester, 1986.
7. Sathyamoorthy, M., 'Nonlinear vibration analysis of plates: A review and survey of current developments', *Applied Mechanics Review* **40**, 1987, 1553–1561.
8. Landa, P. S., *Nonlinear Oscillations and Waves in Dynamical Systems*, Kluwer, Dordrecht, 1996.
9. Landa, P. S., 'Turbulence in nonclosed fluid flows as a noise-induced phase transition', *Europhysics Letters* **36**(b), 1996, 401–406.
10. Landa, P. S., 'What is the turbulence?' (afterward in the paper of Yu. L. Klimontovitch, *Izv. VUZov*), *Prikladnaya Nelineynaya Dinamika* **2**, 1995, 37–41 [in Russian].
11. Guckenheimer, J. and Holmes, P. J., *Nonlinear Oscillations, Dynamical Systems and Bifurcations of Vector Fields*, Springer-Verlag, New York, 1983.
12. Schuster, H. G., *Deterministics Chaos*, Physik-Verlag, Weinheim, 1984.
13. Kuklin, P. M. (ed.), *Selfwaves Processes in the Diffusion Systems*, IPF, Gorkij, ANSSSR, 1981 [in Russian].
14. Stoliarov, N. N. and Riabov, A. A., 'Stability and postcritical behavior of rectangular plates with variable thickness', in *Investigation of Plates Theories*, Kazan, 1982, pp. 195–145 [in Russian].
15. Arnold, V. I., *Ordinary Differential Equations*, Mir, Moscow, 1977 [in Rusian].
16. Arnold, V. I., *Theoretical Problems of Ordinary Differential Equations*, Mir, Moscow, 1978 [in Russian].
17. Babin, A. V. and Vishik, M. N., 'Attractors of the evolutionary partial differential equations and estimation of their dimension', *Uspekhi Matematiceskich Nauk* **38**(4), 1983, 133–187.
18. Krysko, V. A., 'Dynamical stability loss of rectangular shells with finite deflections', *Prikladnaja Mekhanika* **15**(11), 1979, 58–62 [in Russian].
19. Krysko, V. A. and Fedorov, P. B., 'Stability loss of thin comical shells subjected to a heat impact', *Prikladnaja Mekhanika* **16**(5), 1980, 126–129 [in Russian].
20. Krysko, V. A. and Dediukin, I. Ju., 'On the criterions of dynamical stability loss', *Prikladnaja Mekhanika* **30**(10), 1994, 67–71 [in Russian].